Pore Structures and Kinetics of the Thermal Decomposition of $Al(OH)_3$

The isothermal decomposition of gibbsite (aluminum hydroxide) was studied under controlled, pure water vapor pressures from 50 to 3,000 Pa over the temperature range from 458 to 508 K; the effect of sample particle size was also investigated. The partial conversion to boehmite (AlOOH) and the subsequent formation of a ρ-transition alumina product phase were followed with respect to the reactor operating conditions. Nitrogen and water vapor adsorption measurements were used to evaluate the chemical kinetics of the formation of ρ-alumina in terms of an interface velocity, and to interpret the observed dependencies on temperature and water vapor pressure. An adsorption/decomposition model is presented for these kinetics. The interpretation is consistent with the observation that decomposition rate is inversely proportional to the square of the water vapor pressure. The apparent activation energy of 342 ± 15 kJ/mol includes a water adsorption energy, as well as the chemical decomposition contribution of 260 ± 20 kJ/mol.

Lawrence Candela, D. D. Perlmutter
Department of Chemical Engineering
University of Pennsylvania
Philadelphia, PA 19104

Introduction

Because alumina and its partial hydrates are used extensively in technical applications as absorbents, catalysts, and catalyst supports, the thermal decomposition of industrial gibbsite and other crystalline forms of aluminum hydroxide deserves special attention.

There is wide acceptance (Rouquerol et al., 1975; Tertian and Papee, 1958; de Boer et al., 1985a,b; Scott and Horsman, 1970) of the idea that whether heated in air or in water vapor, the first step in the thermal decomposition of $Al(OH)_3$ is a condensation of opposing hydroxyl groups of the layered crystal structure followed by the subsequent internal nucleation and growth of a boehmite phase (AlOOH, also called α-alumina monohydrate). A tight crystal structure and an impeded diffusion of H_2O through the crystal and/or a difficult desorption from the surface is thought to create the high internal water pressure needed for the reaction, since it is known (Wefers and Bell, 1972) that $Al(OH)_3$ can be converted quantitatively to boehmite by hydrothermal treatment in an autoclave or by boiling in alkaline aqueous solutions.

Further indicative of an internal decomposition are the results of Rouquerol et al. (1975) and de Boer et al. (1954b, 1956) showing that the progress of the boehmite formation occurs without any texture modification of the exterior surface and only by the formation of large, inkwell-type pores of low surface area. As the boehmite phase grows, the shell of $Al(OH)_3$ becomes progressively thinner and unable to maintain high water vapor pressures, and the rate of this first decomposition process diminishes. The effect of increasing the particle size of agglomerated crystallites has been recognized to increase boehmite formation (Rouquerol et al., 1975; Tertian and Papee, 1958; de Boer et al., 1954a; Torkar et al., 1961; Sato, 1959; Calvet and Thibon, 1954; Papee and Tertian, 1956; Scott and Horsman, 1970; Wefers and Bell, 1972). This result may be attributed to the greater diffusion distance for water acting to maintain high internal pressure.

The effect on the reaction rate of the atmosphere surrounding the decomposing hydroxides has also been studied (Rouquerol et al., 1975; Tertian and Papee, 1958; Papee and Tertian, 1956; Calvet and Thibon, 1954; Eyraud and Goton, 1954), and the critical importance of the water pressure near the sample has been emphasized. The trend for slower reaction rates and increased boehmite formation at increased partial pressures of water is consistent with the previous ideas; it presumably hinders the desorption of water vapor and its diffusion. This explanation has, however, been criticized by Rouquerol et al. (1975) and by Courtial et al. (1956), who have noted enhanced boehmite yields for thermal treatments at extremely low heating rates over time periods expected to diminish water gradients within the reacting particles.

Variations of these and other operating parameters can

change the extent of the boehmite conversion from zero to about 30%. When boehmite does form, the completion of its formation is generally marked by the abrupt formation of a set of slit-shaped pores parallel to the gibbsite basal planes. Birefringence studies by de Boer et al. (1956) and optical crystallographic methods of Arakelyan and Chistyakova (1962) established that the fissuring occurs uniquely parallel to the (001) crystal faces; no texture changes occur on the hexagonal (001) planes. This fissuring is not accompanied by any intrinsic decomposition process, and thus occurs without any weight loss. De Boer et al. (1954b) and Rouquerol et al. (1975) concur that the internal formation of boehmite pockets and the diffusion of product water vapor across the basal planes act to destabilize the gibbsite structure, which then fissures along its weakest planes. This fissuring phenomenon produces relatively uniform slits of widths near 2.8×10^{-3} microns (μm) in size (de Boer et al., 1956) as determined from nitrogen adsorption hysteresis measurements, and subsequently divides the gibbsite crystal into an array of slablike crystals that are nevertheless internally connected, maintaining the structural integrity of the particle as a whole.

The second decomposition of gibbsite to one of a number of possible lower alumina hydrates follows after the completion of the decomposition to boehmite and fissuring of the remaining gibbsite crystals. It should be noted that kinetic considerations do not actually forbid the simultaneous production of boehmite and ρ-transition alumina in the early stages of the decomposition process. However, the exterior surface available for the decomposition to transition alumina is so small that the yield of this product over the time span in which boehmite production is dominant is quite marginal, even with respect to the sensitivity of nitrogen-adsorption type measurements. The fissuring phenomenon, occurring near the end of the decomposition to boehmite step, greatly enhances the measured conversion rate for the decomposition to ρ-transition alumina, and thus, with respect to various measurement techniques, the decomposition processes appear sequential. Birefringence studies of de Boer et al. (1956) established the direction of movement of the reaction interface as being perpendicular to the newly exposed (001) basal planes; Rouquerol et al. (1979) describe the so-called drilling of micropores in this direction in some detail.

The identity of the product of the second decomposition has been studied using X-ray crystallographic techniques (Tertian and Papee 1953a,b; Tertian et al., 1954). After heating under atmospheric pressure, a phase designated as χ-alumina of molecular formula $Al_2O_3 \cdot 0.6\ H_2O$ was recorded. After heating under low pressures of pure water vapor, a phase designated as ρ-alumina of molecular formula $Al_2O_3 \cdot (0.45\text{–}0.55)\ H_2O$ was seen; heating under high vacuum also produced an alumina with the formula $Al_2O_3 \cdot 0.45\ H_2O$, but it was an amorphous phase. These researchers admitted to some uncertainty in the degrees of hydration quoted. The aluminas produced under low pressure were much more easily rehydratable and were characterized by calorimetry as being strained, high-energy solids.

The various products possible from the second decomposition are highly microporous and possess parallel, cylindrical-type pores of diameters in the range from 5×10^{-4} to 15×10^{-4} μm and BET surface areas from 200 to 300 m^2/g $Al(OH)_3$. Rouquerol et al. (1979) maintained that increasing the water vapor pressure surrounding the decomposing material acted to increase the diameters of these capillary pores. After heating under vacuum, the amorphous product did not possess pores that could be filled with nitrogen adsorbate. For extremely low and carefully controlled decomposition rates, the same authors maintained that the decomposition process was controlled by the desorption of product water vapor from the bottom of the ensuing capillaries. The abnormally high apparent activation energies were consistent with those observed for desorption-controlled dehydroxylations of other layered hydroxides (Brindley et al., 1967a,b).

Despite the extensive prior studies in this area, a full description of the temperature and water vapor pressure effects on the decompositions has not yet been presented, nor has quantitative consideration been given to the degree of fissuring of the gibbsite crystal, its relationship to the extent of the boehmite conversion in the first decomposition, or the nature of the slablike particles it produces. This paper addresses these issues by reporting the results of a systematic study of the pore structures and surfaces that accompany the decomposition of $Al(OH)_3$. Isothermal thermogravimetric analyses over a full range of reactor conditions of temperatures and water vapor pressure are detailed and a kinetic model for the decomposition to ρ-transition alumina is presented and used to interpret the rate data.

Experimental

Samples preparation

Refined crystalline aluminum hydroxide of the gibbsite form was obtained from the Alcoa Chemical Co. It had been produced by precipitation from a hot sodium aluminate solution, with the intention of keeping organic and silicate impurities low. It is designated as Grade C-31 Coarse (by virtue of its relatively large average particle size) and has a pure white appearance. Major impurities are reported to be 0.01% SiO_2, 0.004% Fe_2O_3, 0.2% Na_2O, and 0.04% moisture. The total weight loss resulting from ignition to 1,100°C is 34.5% (theoretical total = 34.64%) and the total Al_2O_3 content is reported as 64.90% (theoretical total = 65.36%).

Tyler U.S. Standard testing sieves (38–180 μm sizes) were used to separate the aluminum hydroxide into a series of particle size fractions. Under a high-resolution optical microscope, the aluminum hydroxide particles appear as fused aggregates of smaller tabular and prismatic crystals, the pseudohexagonal crystal habit being displayed quite distinctly.

A sample in the 75–88 μm sieve range was analyzed on a Norelco diffractometer using the Cu $K\alpha_1$ emission of wavelength 1.5405×10^{-4} μm. The crystallographic distances and the intensity ratios obtained from the major peaks of the X-ray diffraction pattern are given in Table 1, where they are compared with the ASTM standard. There was no evidence in the X-ray pattern of the presence of any other alumina phase.

Nitrogen adsorption measurements at 77 K were made on a sample in the 38–45 μm sieve range. A BET analysis resulted in a surface area of 0.25 m^2/g $Al(OH)_3$. This low figure and the lack of any adsorption/desorption hysteresis indicate a lack of significant porosity.

Thermal analyses

The kinetics of the thermal transformations studied were measured by recording weight losses during the various dehydration processes on a Cahn System 2000 Recording Electrobalance. Most of the thermal treatments were performed on gibb-

Table 1. Comparison of X-Ray Diffractometer Results of Reactant Gibbsite and Product Boehmite with their ASTM Standard Values

Gibbsite Reactant				Boehmite Peaks in Product Phases			
Experimental		ASTM Standard		Experimental		ASTM Standard	
d, $10^{-4}\mu m$	I/I_o	d, $10^{-4}\mu m$	I/I_o	d, $10^{-4}\mu m$	I/I_o	d, $10^{-4}\mu m$	I/I_o
4.88	1.00	4.82	1.00	6.20	1.00	6.11	1.00
4.39	0.43	4.34	0.40	3.20	*	3.16	0.65
4.35	0.18	4.30	0.20	2.36	0.60	2.34	0.55
3.32	0.10	3.31	0.06	2.06	*	1.98	0.06
2.46	0.16	2.44	0.16	1.87	0.36	1.86	0.30
2.39	0.20	2.37	0.20	1.86	0.32	1.85	0.25
2.06	0.15	1.98	0.10	1.77	0.10	1.77	0.06
1.81	0.11	1.79	0.10	1.66	0.20	1.66	0.14
1.76	0.11	1.74	0.10	1.53	0.07	1.53	0.06
1.69	0.10	1.67	0.10	1.461	*	1.45	0.16
—	—	—	—	1.458	*	1.43	0.10

*These intensities were abnormally increased due to overlap with other phases.

site samples near 10 mg in size. The particles were spread in a thin layer in the open platinum pan and were suspended by a thin nichrome wire about 2 ft (0.6 m) below one arm of the electrobalance; the beds were generally from one to two particles in thickness. These conditions were employed to minimize thermal and material transport resistances, however, tests of much greater bed depth also usually gave identical results. The entire assembly was contained in a vacuum bottle for air evacuation. The platinum boat and sample were positioned at the center of an exterior cylindrical resistance furnace. The process temperature was measured with an alumel-chromel thermocouple positioned close to the reacting sample, and the heating programs used PID closed-loop control to maintain temperatures to within ± 0.5 K.

Because of thermal lags during heating and self-cooling caused by the endothermic decompositions, calculations were performed to estimate the deviation between the sample temperature and the reactor temperature as measured by the thermocouple. Worst-case estimates showed that the maximum possible temperature lag experienced while executing heating ramps was less than 2 K. Even during the most rapid thermal decompositions, self-cooling was unlikely to exceed 0.2 K, a deviation that is less than can be detected with the sensitivity of the alumel-chromel thermocouple.

Since the micropores that form during the decomposition to transition aluminas are close in size to the molecular diameters of nitrogen and oxygen, diffusional resistances for product water vapor could be appreciable in a mixed gas. To avoid this possible complication, and to guarantee that the local vapor pressure at dehydroxylation sites could be closely controlled, pure water vapor atmospheres were employed, supplied to the system by pumping out the air and opening to a reservoir of distilled water or a saturated solution of $CaCl_2 \cdot 6H_2O$. The water pressure is thus controlled by a thermostatically controlled bath, using the data of Washburn (1928) for vapor pressure over these salt solutions. The water vapor pressure was varied from 50 to 3,200 Pa, and the precision of the Setra Electronic Manometer display was ± 4 Pa.

System preparations included several vacuum evacuations and pure water vapor purges in order to insure a pure reactor atmosphere. After pressures equilibrated, the gibbsite samples were outgassed of their adsorbed gas constituents by heating to 423 K. Laubengayer and Weisz (1943) showed this temperature to be comfortably below the limit for gibbsite stability; after about 2,000 s, samples were usually completely outgassed and a constant, dry weight baseline could be measured. For the isothermal investigations used here, samples were heated rapidly to the desired process temperature. Ramp times were normally 600 to 700 s and did not overlap the section of the TGA scan for the decomposition to transition alumina; overlaps with the first thermal decomposition to boehmite were usually small compared with the total time for this process. Isothermal conditions were thus maintained throughout the entire time of the second decomposition.

Gas adsorption

Nitrogen adsorption measurements, using a Quantachrome Quantasorb instrument, were used for surface area and pore structure determinations of powdered samples. This system employs digital gas flow controllers for accurate mixing of tanked, high-purity adsorbate (here N_2) and carrier gas (here He), providing full-range variability in the adsorbate gas mole fraction and hence in its relative pressure. The gases were further purified using a liquid nitrogen cold trap. Water vapor, adsorbed from the atmosphere, was the major surface contaminant and had to be thoroughly removed during outgassing.

The specific surface areas of the samples were determined from the nitrogen isotherms using a standard BET analysis. Additionally the shape of the nitrogen adsorption/desorption hysteresis loop can also yield information on the geometry and nature of the pore structure of the investigated material. By classifying isotherm shapes DeBoer and Lippens (1964a) have shown how to distinguish between those arising from cylindrical-type pore systems and those arising from slit-shaped pores.

Once the pore geometry has been determined, the pore size distribution and the cumulative pore surface area can be extracted from the relevant arm of the N_2 adsorption/desorption isotherm. A numerical technique similar to that of Barrett et al. (1951) was employed here for cylindrical pore systems and the method of Lippens et al. (1964) was used when slit pores predominated. If the pore system has a cylindrical inkwell-type character (wide interior gaps connected to the particle surface via narrow necks), de Boer et al. (1964b) contend that the pore size distribution analysis must be based on the adsorption arm of the hysteresis loop, whereas for systems of more uniform pore dimensions, the desorption arm information is more relevant to the operating equilibrium phenomenon.

The numerical procedures used for the pore size distribution analyses were based on the Kelvin equation

$$\ln P/P_o = \frac{-2\gamma V_m \cos\alpha}{RT r_k} \tag{1}$$

which relates the relative pressure of the adsorbate to the surface tension of the adsorbate at its boiling point, the molar volume of liquid adsorbate, the adsorbate wetting angle, and the Kelvin radius of the capillary or pore. At $P/P_o = 1$, all pores are completely filled with adsorbate due to capillary condensation. As one moves along the relevant isotherm arm to lower relative pressure values, the largest pores begin emptying, as determined

by the Kelvin equation. At a given relative pressure, all pores smaller than the associated Kelvin radius remain filled whereas all pores larger have only an adsorbed layer.

This method is useful in determining information on the pore structure for the interval of pore sizes between about 18 and 200×10^{-4} μm. The Kelvin equation indicates that the information on pore sizes greater than 200×10^{-4} μm is contained in the isotherm between relative pressures of about 0.96 and 1.0. This segment is small and precision tends to be poorer than at lower relative pressures. The information on pores with diameters less than 18×10^{-4} μm is contained at relative pressures less than about 0.30. Because the Kelvin equation is intended for systems of macroscopic scale, its usefulness is questionable for treating capillaries of only a few molecules in size. Adsorbed monolayers will completely fill pores in this circumstance and adsorption hysteresis will not occur. As a result, if a material has significant pore area below 18×10^{-4} μm, its magnitude is taken as the difference between the BET area and the cumulative pore area from the Kelvin analysis. Pores above 200×10^{-4} μm do not contribute significantly to the total pore area for these cases.

Further adsorption measurements using H_2O as the adsorbate were made gravimetrically on the thermal assembly. Relevant pore structure information was determined in a similar manner as for the nitrogen adsorption, but with the system constants appropriate for water vapor.

Results and Discussion

Decomposition to boehmite

A typical weight-loss curve for the isothermal decomposition of gibbsite is illustrated in Figure 1. This particular example is for a 63–75 μm particle size fraction decomposed at 498 K under a water vapor pressure of 370 Pa. The first decomposition of gibbsite to boehmite (AlOOH) shows up below the first inflection in the weight loss plot, and is the unique chemical transformation occurring for most of this region. The progress of this reaction was additionally monitored using X-ray diffraction techniques; an example of *d*-spacing and intensity results for the boehmite phase is provided in Table 1. The conversion of the gibbsite to boehmite is only partial and the rate of its conversion generally decreases as its final level is approached. The second decomposition of the remaining gibbsite to a poorly defined transition alumina ($Al_2O_3 \cdot xH_2O$) ensues directly and the rate of the sample's weight loss accelerates. Both processes overlap somewhat and an inflection point in the weight loss scan is usually distinct. The rate of weight loss during the second decomposition remains constant for a large portion of the reaction and finally decelerates as the last of the gibbsite reactant is consumed.

From reactions wholly within the regime of decomposition of gibbsite to boehmite, there developed wide, sloping nitrogen isotherms of the type D category of de Boer (1958). These are indicative of inkwell-type pore structures, reported by several investigators to occur during the intragranular formation of boehmite within the gibbsite crystals. Capillary-based, adsorption-arm calculations resulted in wide distributions of capillary sizes from 20 to 200×10^{-4} μm and beyond. The cumulative pore surface areas compared well with the results from BET analyses and supported the claim that the boehmite formation was the unique chemical reaction in progress. For samples in the 63–75 μm sieve range, inkwell pores areas at complete conversion ranged from 3 to 5 m^2/g $Al(OH)_3$ for a variety of thermal treatment conditions. These low surface area figures are consistent with the findings of de Boer et al. (1956) and Rouquerol et al. (1975).

Decomposition to transition alumina

Pore Structures. The development of the slit-shaped pores, caused by the fracturing of the gibbsite crystals parallel to their (001) planes, and of the cylindrical micropores accompanying the decomposition to transition alumina were both studied.

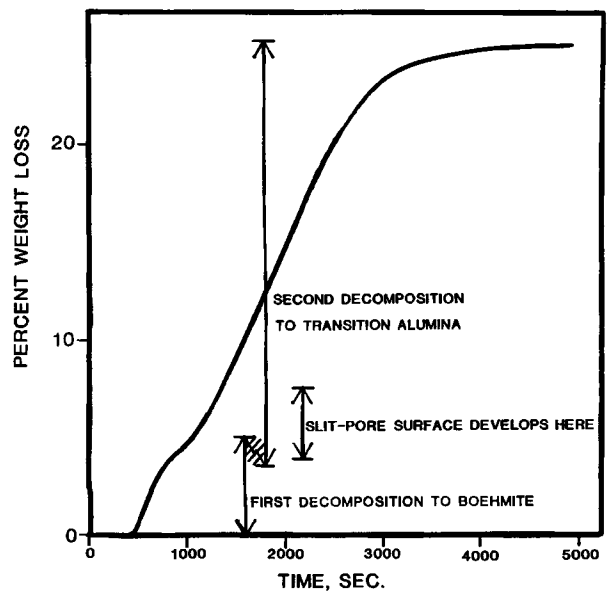

Figure 1. Typical thermal composition weight loss diagram.

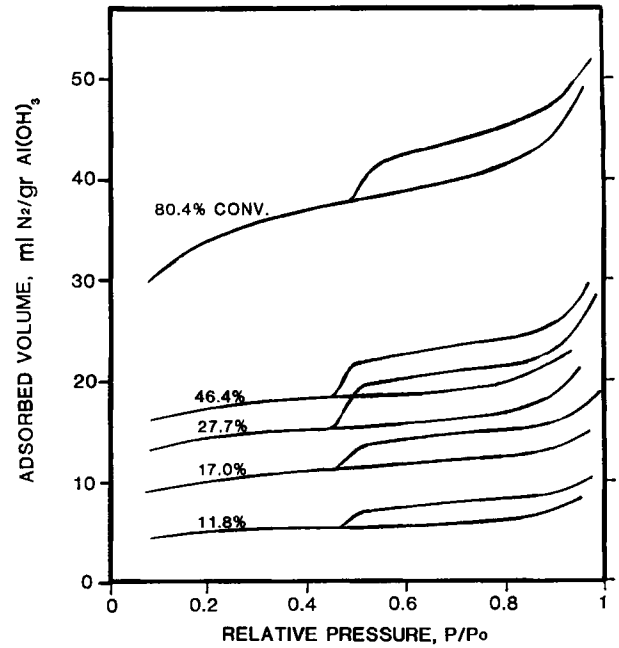

Figure 2. Nitrogen adsorption isotherms for various degrees of conversion during second decomposition.

Samples were decomposed to several levels of conversion within the regime of the second decomposition process and the complete nitrogen isotherms were measured and analyzed. Figure 2 illustrates these results for samples decomposed isothermally at 478 K under a pressure of 273 Pa of water vapor. The hystereses measured were clearly of the type B classification of de Boer (1958) for parallel slit-shaped pores open on all sides. The increase in the adsorption capacity with the increase in the conversion was indicative of the porosity of the transition alumina secondary decomposition product. The increase in the width of the hysteresis gaps indicates an increase in the number of slit pores.

Figure 3 shows the development of both the capillary surface area and the slit-pore area as a function of the percent conversion to transition alumina of the gibbsite that was unconverted to boehmite. The values shown for the slit pore area were obtained from the cumulative pore area plots in the interval of relative pressures from about 0.40 to 0.65, or from the corresponding slit pore diameters from about 24 to 35×10^{-4} μm. In all cases, a sharp peak in the distributions was found near 28×10^{-4} μm, consistent with the results of previous researchers. The cumulative area for pore sizes greater than 35×10^{-4} μm was always near the BET results referred to above as the inkwell pores of the primary decomposition to boehmite. The 35×10^{-4} μm dividing line for the two pore structures is somewhat arbitrary given the continuous nature of the distribution, yet it seems to mark where the peak in the distribution begins to rise abruptly from the comparatively featureless region at greater diameters. It also served to standardize the analyses for a large data set. The developing capillary pore structure consisted of pores smaller than 18×10^{-4} μm dia. and is thus not included in the cumulative pore analysis.

Figure 3 shows that the capillary surface area rises linearly with the percent conversion, consistent with the Rouquerol (1979) model of micropores drilling perpendicularly into the (001) gibbsite crystal faces. The slit pore surface area also rises rapidly with conversion but then levels off to a constant value. The zone in which the slit pore area is increasing corresponds to

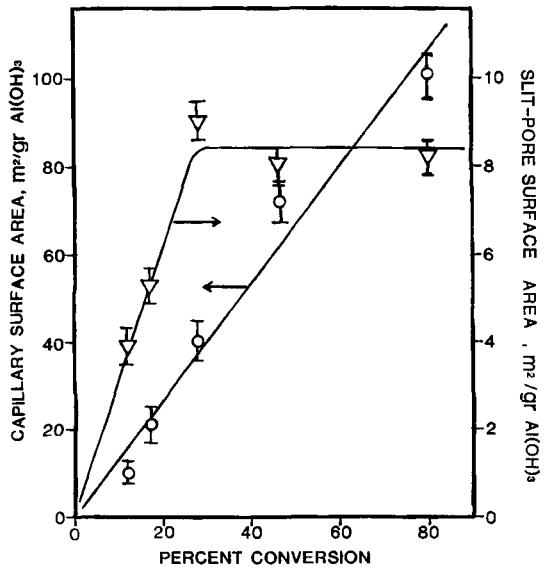

Figure 3. Surface area contributions at various degrees of conversion for second decomposition.

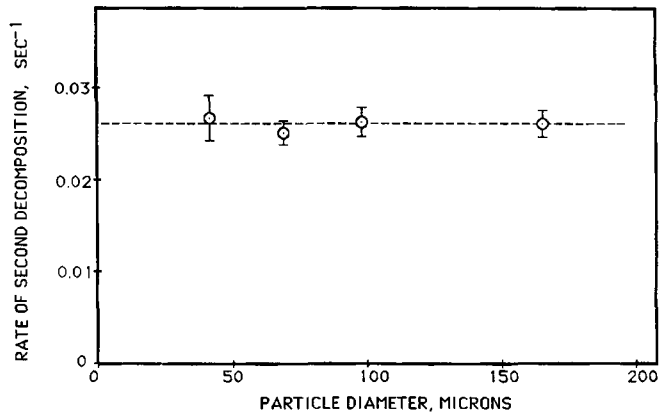

Figure 4. Effect of particle size on rate of second decomposition.

the segment of the TGA weight loss curve in Figure 1 just past the inflection point marking the end of the primary decomposition to boehmite. The rate of the decomposition to transition alumina accelerates as the slit pore area increases and reaches its constant value just as the slit pore area levels off. This suggests that the rate of the decomposition to transition alumina is proportional to the surface that is exposed during the fracturing of the gibbsite crystals, a finding consistent with the idea that the fracturing exposes the planes perpendicular to which the second decomposition is known to proceed.

Figure 4 shows that the kinetics of the decomposition to transition alumina are independent of particle size for isothermal

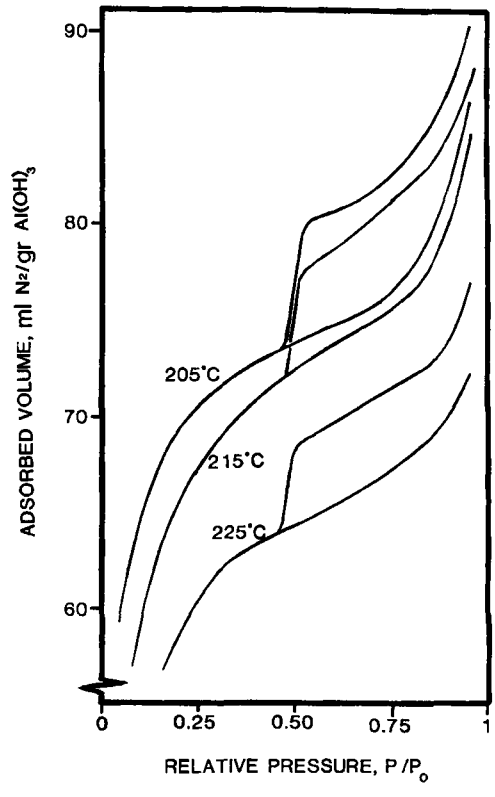

Figure 5. Nitrogen adsorption isotherms as a function of decomposition temperature.

treatment at 508 K under 1,400 Pa water vapor pressure. This evidence argues against the possibility that the rate of this decomposition could be independent of the degree of splitting of the gibbsite crystals, since if that were the case one would expect the measured kinetics to be strongly influenced by the particle size of the sample such that the exterior surface would govern the interface between the product and the reactant. For spherical particles, for example, the initial rate of decomposition would be inversely proportional to the particle diameter, clearly not the behavior shown in Figure 4.

Measurements of the slit pore and capillary surface areas were also made for fully decomposed gibbsite samples treated under a variety of TGA conditions. Figure 5 compares the nitrogen isotherms of samples decomposed at 800 Pa water vapor pressure at different reactor temperatures. As presented in Table 2, the slit areas and capillary areas both rise moderately as reactor temperature is decreased. The trend for larger slit areas at lower temperatures may be explained by noting that higher boehmite conversions also accompany lower temperature treatments. The greater conversion to boehmite destabilizes the gibbsite crystal and enhances fracturing. Pore widths of the capillaries produced are known to be affected by reactor conditions; Rouquerol et al. (1979) noted wider pores for treatment at increased water vapor pressures. The trend for enhanced adsorption capacity at lower operating temperatures and fixed water vapor pressures, as reflected by the trend in capillary surface areas, is probably also due to a slight enhancement in the capillary diameters.

Figure 6 compares the nitrogen isotherms for a number of different TGA reactor conditions; in these cases, the water vapor pressure and temperature were progressively increased while the linear conversion rates of the decomposition to transition alumina were held constant at about 0.013% conv/s.

The drastic increase in the adsorption capacity from 140 to 800 Pa water vapor pressure is due to an increase in the crystallinity of the decomposition product, known to enhance the porosity (Young, 1966) available to absorbates. Rouquerol et al. (1979) obtained a completely amorphous decomposition product at 5.3 Pa water vapor pressure that was nonporous with respect to nitrogen adsorbate. At 133 Pa, a ρ-alumina phase was produced that had an adsorption capacity of the order found here.

Figure 7 also compares the BET capillary surface areas obtained by using nitrogen and water vapor adsorbates as a function of the operating water vapor pressure during the thermal analyses. As shown, the capillary area available to nitrogen dropped off rapidly at low TGA operating water vapor pressures, whereas the area available to water adsorbate changed relatively little across the full span shown. Furthermore, the volumetric filling of nitrogen and water adsorbate was similar for the higher pressure conditions, even though the adsorption of H_2O was almost twice that of N_2 on a molar basis.

Interpreting this information in terms of steric limitations to adsorption suggests that the diameters of the microcapillaries

Table 2. Slit Pore and Capillary Surface Areas for Fully Decomposed Gibbsite Samples

	Slit Area		Capillary Area	
Temp. K	m^2/g init. $Al(OH)_3$	m^2/g $Al(OH)_3$ unconv. to boehmite	m^2/g init. $Al(OH)_3$	m^2/g $Al(OH)_3$ unconv. to boehmite
478	14.0	17.7	219	280
488	12.3	15.3	207	260
498	10.2	12.4	177	219

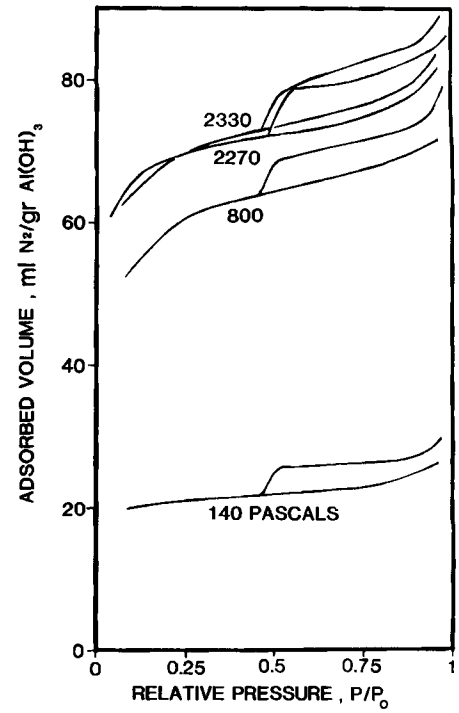

Figure 6. Nitrogen adsorption isotherms as a function of water vapor pressure during decomposition.

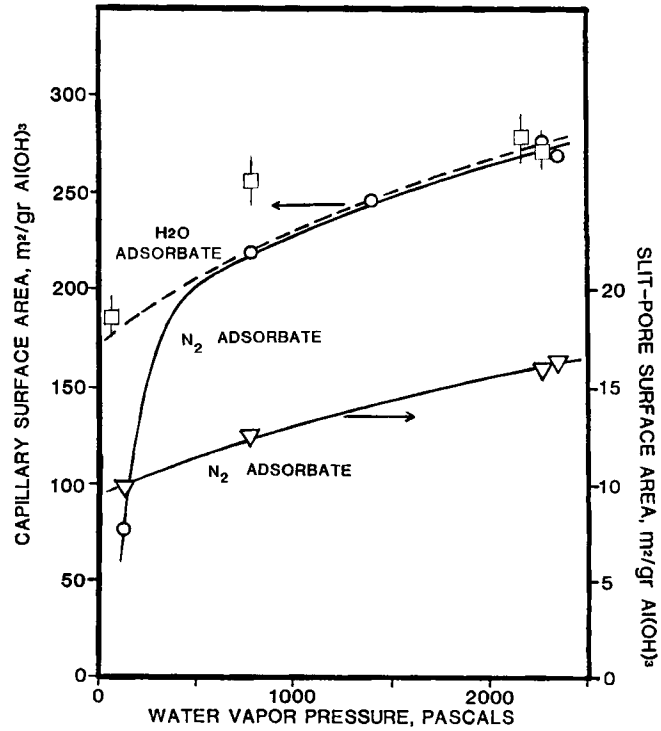

Figure 7. Surface area contributions as a function of water vapor pressure during decomposition.

forming during the decomposition to transition alumina varied from about 4 to 6 $\times 10^{-4}$ μm as the TGA water vapor pressure was increased in the thermal analyses. Figure 8 illustrates that even though a nitrogen molecule of length 4.2 $\times 10^{-4}$ μm and width 3.1 $\times 10^{-4}$ μm (Pauling, 1960) could be sterically hindered from entering a small capillary, two water molecules of diameter 2.8 $\times 10^{-4}$ μm (Morgan and Warren, 1938) could still adsorb with only a slight overlap. Two water molecules will even more readily fit into the larger 6.0 $\times 10^{-4}$ μm capillaries, while nitrogen would be expected to adsorb singly.

The differences among the nitrogen isotherms at higher water vapor pressures are relatively small. The slit pore and capillary surface areas were found to increase gradually with increasing water vapor pressure. This enhancement of the slit pore area is correlated very well to the enhanced boehmite conversions also seen at increasing water vapor pressures and is consistent with the idea that the boehmite conversion in the first decomposition process controls the degree to which the gibbsite crystals split along their basal planes. The gradual enhancement of the capillary area with increasing water vapor pressure is due to a widening of the capillary diameters as measured by Rouquerol et al. (1979).

In Figure 7, the capillary surface areas and slit pore surface areas are expressed in units of m^2 per gram of gibbsite not consumed in the first decomposition. Since the conversion to boehmite in the first decomposition varies for different reactor conditions, the proper basis for the surface area contributions (and for subsequent decomposition kinetics) for the decomposition to transition alumina is this renormalized one. Since the conversion to boehmite is increased by increasing the particle size of the gibbsite reactant, it would be misleading to compare the 63–75 μm cases with the 150–180 μm case when discussing the slit pore area. It is acceptable however to mix these different particle size cases when discussing the capillary area, since this latter measure is completely independent of the boehmite conversion.

Thermal Analyses. A full set of isothermal decompositions was performed on gibbsite samples in the 63–75 μm sieve range. System water vapor pressures (and total pressures) were studied from 50 to 3,200 Pa and furnace temperatures were varied from 458 to 508 K. The rates of the decomposition to transition alumina were determined from the linear portion of the weight loss scans and are presented in Figure 9. On the logarithmic coordinates used the conversion rates vary linearly with water vapor pressure at each temperature. A least-squares analysis was performed on each of the six isothermal data sets, yielding slopes that demonstrated no trend with temperature. Accordingly, a set of parallel lines is shown on Figure 9 with average slope of -1.83 ± 0.13 (95% confidence limits).

In determining the rate of the decomposition to transition alumina, it was necessary to estimate independently the extent of the partial conversion to boehmite. Differential scanning calorimetry (DSC) was performed on several fully decomposed samples. The peak in the scan near 830 K (heating rate = 0.333 K/s), corresponding to the dehydroxylation of the boehmite, was measured for comparison to the peak of a pure boehmite reference sample. Figure 10 illustrates the matched peak positions and overall shape of the scans. Pseudoboehmite constituents, which typically decompose well below 800 K, appear to be minimal in all cases. The different baseline slopes of the two scans of Figure 10 are a consequence of small changes in instrument settings. Independently, the DSC results were consistent with measurements of the boehmite conversion levels obtained through calibration of peak intensities on an X-ray diffractometer. The results indicated that the conversion to boehmite ceased just below the inflection point in the TGA scan, the level that effectively separates the first and second decomposition processes.

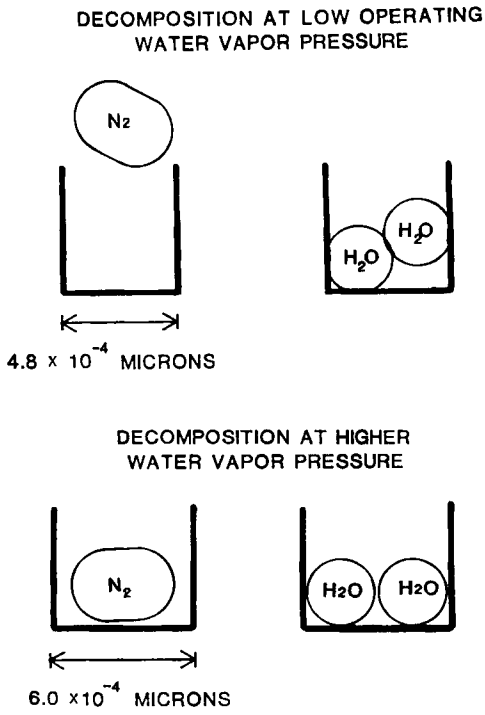

Figure 8. Nitrogen and water adsorption in microcapillaries.

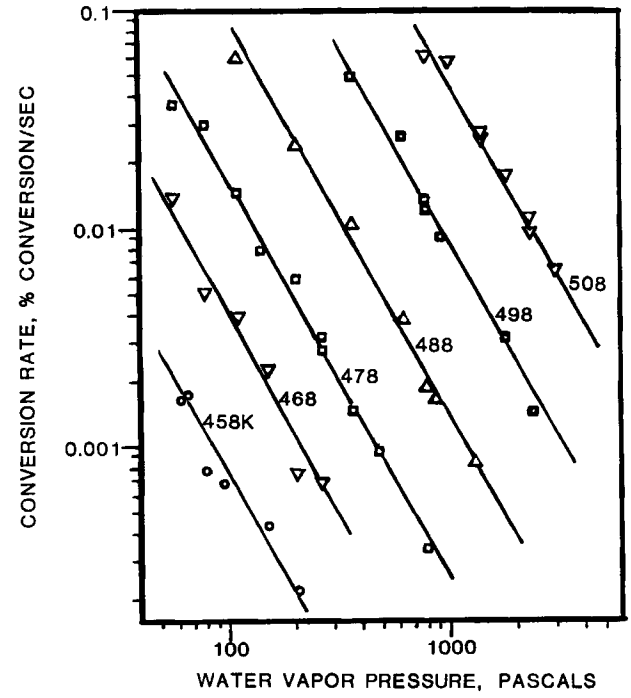

Figure 9. Conversion rates for second decomposition to transition alumina.

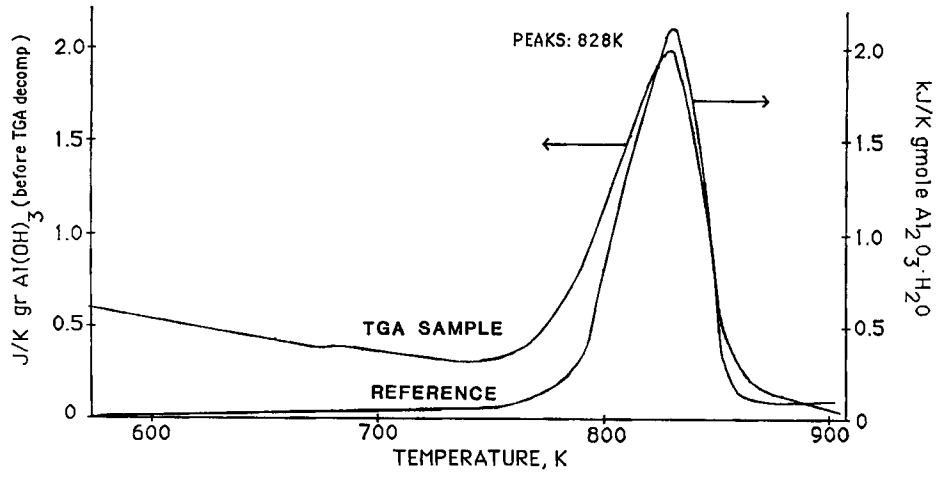

Figure 10. Comparison of differential scanning calorimetry traces.

Figure 11 superimposes the boehmite conversion level results on the TGA data in which water vapor pressure and thermal operating parameters were varied. As shown, conversion to boehmite at any given temperature is enhanced by increasing the water vapor pressure. At constant water vapor pressure, increasing the operating temperature diminishes the conversion to boehmite. These results are consistent with those of previous investigators. Rouquerol et al. (1975), working with a constant rate thermal analyzer and operating under pure water vapor atmospheres, also noted enhanced boehmite conversions with increasing PH_2O. They also noted higher boehmite conversions accompanying lower heating rate analyses, in agreement with findings reported in Figure 11 for isothermal treatment at decreasing temperatures.

For thermal treatment under atmospheric pressure, Wefers and Bell (1972) reported enhanced boehmite formation with increasing PH_2O, but diminished boehmite formations with lower heating rates. This was in conflict with the findings of Courtial et al. (1956), who found enhanced boehmite conversions for slower heating rates under atmospheric pressure. For isothermal treatment, Papee and Tertian (1956) and Tertian and Papee (1958) reported greater boehmite formation under dry air at atmospheric pressure than for treatment under vacuum, possibly as a result of a small accumulation of product water vapor near the sample.

In general, the overall shape of the weight loss scan for the decomposition to boehmite showed very little sensitivity to changes in the water vapor pressure for fixed-temperature

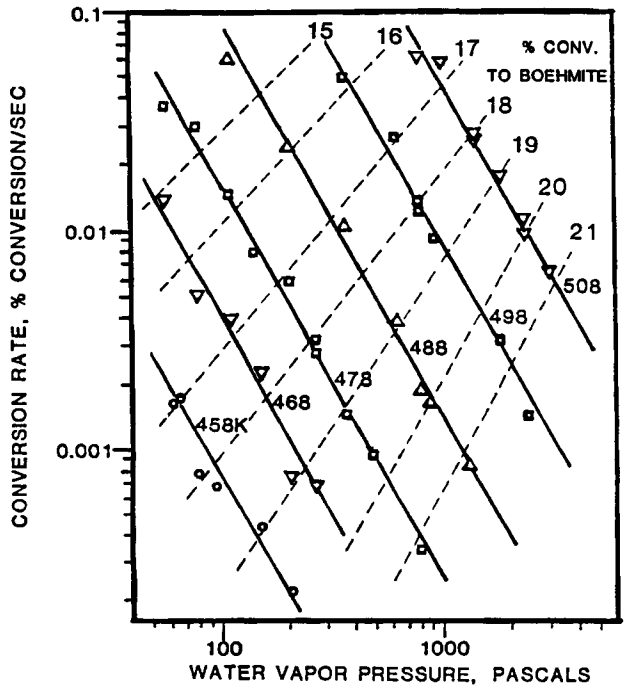

Figure 11. Conversion rates for second decomposition to transition alumina, boehmite conversion levels superimposed.

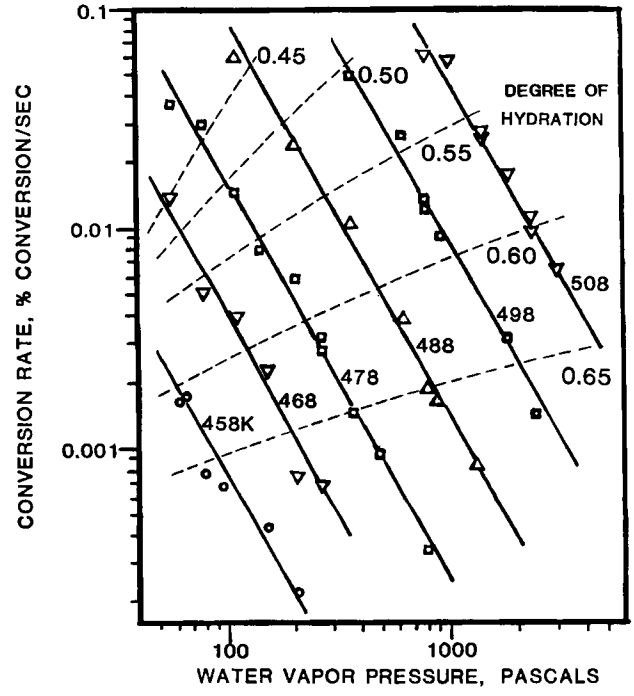

Figure 12. Conversion rates for second decomposition to transition alumina, extent of hydration levels superimposed.

experiments. The level of conversion to boehmite is apparently controlled by the fissuring process that divides the two decompositions. At increasing water vapor pressure, this fissuring occurred later and thus promoted higher boehmite conversions.

The constitution of the alumina product of the second decomposition is also sensitive to the reaction conditions. Written as an alumina hydrate, $Al_2O_3 \cdot xH_2O$, values of the degree of hydration, x, have been reported from about 0.45 to about 0.65. Papee and Tertian (1956) and Tertian and Papee (1958) distinguished between two transition aluminas. One, designated χ-alumina, resulted from isothermal treatment at 523 K under dry air at atmospheric pressure and had a degree of hydration near 0.60. The other, designated ρ-alumina, resulted from isothermal treatment at 453 K under a forced vacuum and had a degree of hydration near 0.50. The ρ-alumina was described as a badly organized, energy-rich solid, consistent with the finding of Calvet and Thibon (1954) that this product had a much higher capacity for rehydration than the χ-alumina. Rouquerol et al. (1979) reported somewhat different results; for pure water vapor atmospheres under 5 Pa, a completely amorphous alumina phase resulted, whereas under 133 Pa, the ρ-alumina was the product as identified by its one peak X-ray pattern at 1.395×10^{-4} μm. Heating under atmospheric pressure resulted in the χ-alumina phase.

Figure 12 superimposes degree of hydration values on the *TGA* data set. These curves were interpolated among the values determined for each experimental data point. The results are consistent with those found in the literature sources. The X-ray pattern of the product of the second decomposition here displayed a weak intensity near 1.39×10^{-4} μm indicative of a ρ-alumina phase. No intensities indicative of the χ-alumina phase were detected when patterns for boehmite and gibbsite were combined.

Transport considerations

In order to correctly interpret the measured overall kinetics, it is necessary to consider the mass transport of the product water vapor as it is emitted by the decomposing gibbsite particle. The first decomposition of the gibbsite produces a boehmite phase that is well dispersed throughout the residual $Al(OH)_3$ and that is accompanied by the formation of pores of diameters greater than about 200×10^{-4} μm. This pore structure forms because the boehmite phase is denser than the parent gibbsite phase; the resulting porosity for this macroporous formation is dependent upon the boehmite conversion level and is between 0.06 and 0.08 for the cases studied here. The microporous slits (dia. = 28×10^{-4} μm) that develop during the transition between the two decomposition processes contribute a porosity from 0.02 to 0.05, and the microporous capillaries (dia. = $5\text{–}10 \times 10^{-4}$ μm) associated with the decomposition to transition alumina contribute a porosity from 0.2 to 0.3. Thus, during the decomposition to transition alumina, after the slit pore structure is fully developed, a product water vapor molecule must diffuse through the capillary in which it was produced to a slit pore, and from the slit pore to a macropore, and then finally out of the particle.

Since the reactor system used here employed a pure water vapor atmosphere, the entire sequence is composed of a series of Knudsen flow processes. The pressure drops associated with the flows through each of the pore systems described were calculated for the most rapid decomposition rates experienced in the experiments. Additionally, system parameters were conservatively estimated in order to give an upper limit on the calculated pressure drops. Thus, a maximum value for the overall pressure drop between the particle center and the exterior atmosphere was sought in order to assess whether or not diffusional resistances were negligible.

The Knudsen diffusion equation was used to calculate the diffusivities associated with the different pore structures, an application justified for the extremely small micropores involved as established by numerous earlier works. Omata and Brown (1972) found, for example, that the regular Knudsen diffusion equation gave either accurate or underestimated diffusivities for a variety of microporous materials, including aluminas. Rao and Smith (1963) obtained good results using this equation to describe hydrogen diffusion through microporous alumina and silica. Gilliand et al. (1958) found that the Knudsen diffusion equation tended to underestimate the diffusion through microporous solids for gases that were able to adsorb onto the solid material, since the equation neglects surface mobility. Alumina and its partial hydrates are good adsorbents for water. Hence, the use of the Knudsen diffusion equation is justified and will, if anything, be conservative in estimating the mass diffusivities here.

The results of these calculations for the conditions which tended to maximize the pressure drops (high decomposition rate, low boehmite conversion and hence, low macroporosities) were:

$$\Delta P \text{ capillary} \simeq 10^{-4} \text{ Pa}$$

$$\Delta P \text{ slit} \simeq 0.1 \text{ Pa}$$

$$\Delta P \text{ macropore} \simeq 5\text{–}10 \text{ Pa}$$

These figures indicate that if diffusion resistances were at all significant, they would only affect the data for runs at very low pressures and very high decomposition rates, situations at the extreme upper left of Figure 9. A pressure drop of 10 Pa is small compared with most of the operating pressures used here. Furthermore, the data at the upper left of Figure 9 compare well with the data at rates that are about three orders of magnitude lower and in which the maximum pressure drop would likewise be about three orders of magnitude lower than 10 Pa, that is, 0.01 Pa. Experiments were performed for reactor conditions that lay well above the data of Figure 9. In these cases, decomposition rates were distinctly suppressed in comparison and indicated the onset of the influence of diffusional resistances.

The decomposition to transition alumina was noted to be largely independent of the gibbsite particle size, and the average particle diameter was increased from 40 to 165 μm without any rate suppression caused by the development of a high internal water vapor pressure. Since Darcy's equation predicts that the overall pressure drop would be proportional to the square of the particle diameter when holding the decomposition rate constant, this evidence suggests that the macropore contribution to the water vapor pressure drop, though the single largest pressure drop contribution, is still of negligible proportions.

The linear dependence of conversion on time for the decomposition to transition alumina is not, of itself, convincing evidence of chemical kinetic control, since Sohn and Szekely (1972) showed that gas/solid reaction involving porous reactants can often display such linear behavior under conditions other than pure chemical kinetic control. In their work, they defined mass

transfer Biot numbers for grains and for the overall pellets comprising a porous solid reactant. They established that their pellet Biot number must be below 0.1 and their grain Biot number below 1.0 in order to be able to ignore diffusional resistance in gas/solid reactions. Since the macropore diffusion resistance has already been shown to be negligible by virtue of the independence of the decomposition rate with respect to particle size, the slabs of decomposing gibbsite formed during the formation of the slit pores can be considered to be analogous to the grains in the model by Sohn and Szekely. Likewise, the stacks of these slabs can be considered to be analogous to Sohn and Szekely's pellet. Calculations of the experimental pellet and grain Biot numbers were found to be of the order of 10^{-4} and 10^{-11}, respectively, very much below the limits calculated by Sohn and Szekely. Hence, particle, subpellet, and grain diffusion limitations are all shown to be negligible by this alternative method.

Further, estimates of the activation energies calculated from the data of Figure 9 are about 330 to 360 kJ/gmol. These values are extremely high, near the upper limit for activation energies normally encountered in chemical kinetics. Strong diffusion limitations would suppress the measured value for the activation energy by half of its value under purely chemical kinetic control. Hence, if diffusional resistances were important, the true value of the activation energy for the chemical decomposition would have to be twice an already very large value.

Thus, two separate calculations estimating diffusional resistances and observations on the nature of the activation energy, the overall trends in the data set, the reduced time plots, and the effect of increasing particle sizes all support the view that gas phase diffusional resistances can be safely ignored for the decomposition to transition alumina.

Kinetics of interface advancement

The kinetics of the decomposition to transition alumina have to this point been expressed in terms of percent conversion per unit time. Since it is known that this decomposition proceeds perpendicularly against the crystal planes exposed during the slit pore formation, a more fundamental expression for the chemical kinetics would be in terms of the velocity of this interface advancement, that is, in units of length per unit time.

The measurements of the slit pore area described above were performed on samples for which thermal decomposition was studied over a full range of reactor conditions, specifically temperature, decomposition rate, and water vapor pressure. The values of the slit pore area were found to increase gradually with increasing water vapor pressure and decreasing decomposition rate. In fact, the trends seen were identical to the trends for the boehmite conversion levels, and the two quantities were well-correlated by the equation:

$$s = 0.0289\, p^{2.11} \tag{2}$$

where s is the slit pore area in m^2/g of $Al(OH)_3$ not converted to boehmite, and p is the percent conversion to boehmite.

This empirical expression was used to transform the contour lines of boehmite conversion given in Figure 11 into contour lines in terms of slit pore area. The values for the slit pore areas for the particular data points in Figure 11 were then obtained by interpolation between the contour lines. The kinetic data of Figure 9 were then reexpressed in terms of the more fundamental interface velocities by use of the equation

$$v = \frac{c}{S\rho} \tag{3}$$

The results are given in Figure 13 as a function of water vapor pressure for a range of reactor temperature conditions. The most important feature of this new representation is the more negative slope of the straight lines through the isothermal data points. No trends of increasing or decreasing slopes were observed as temperature was increased, and a least-squares analysis gives the average slope as -2.12 ± 0.17, where the quoted uncertainty represents a 95% confidence interval over the data scatter. The straight lines of Figure 13 were drawn with a constant slope of -2.0, for reasons described in the following section.

Influence of water vapor on the chemical kinetics

The kinetics of the diffusion of the escaping product water vapor were shown to be rapid in comparison with the chemical kinetics. X-ray crystallographic examinations of fully decomposed samples that had been exposed to a variety of reactor temperatures and water vapor pressures failed to show recrystallization of any $Al(OH)_3$ phases, indicating that the decomposition is an irreversible process for the reactor conditions used here. Thus, mass action and diffusion resistances are negligible and cannot, of themselves, create a dependence of the overall kinetics on the concentration of the product water vapor. The water vapor pressure effect can be explained, however, if the existence of an adsorbed water phase on the reaction sites can suppress the decomposition process. Indeed, Young (1966) notes that water

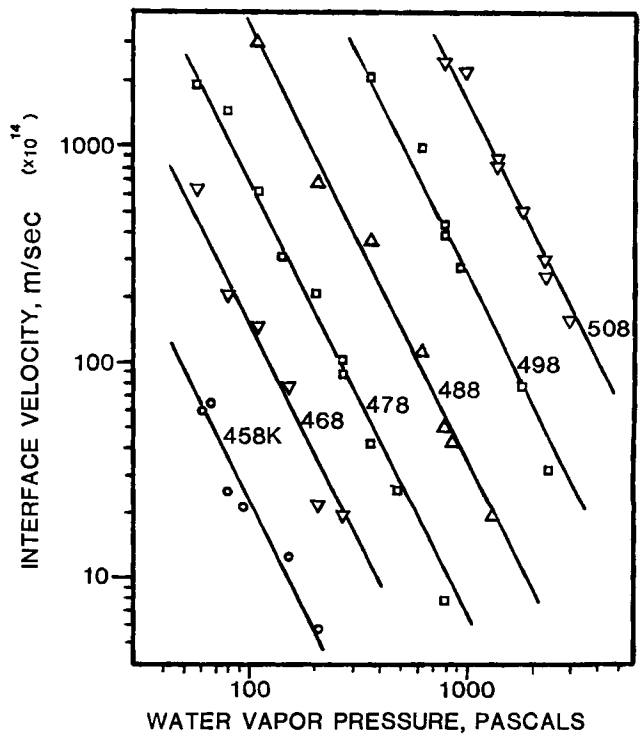

Figure 13. Interface velocities for second decomposition to transition alumina.

molecules adsorbed onto the surface of a disordered ionic solid can either enhance or retard lattice mobility, and can thus have a profound effect on measured chemical kinetics.

A retardation of dehydration caused by the blocking of active areas in the interface region by adsorbed water has previously been proposed by researchers investigating other chemical systems. Acock et al. (1947) utilized a Langmuirian adsorption isotherm to describe the reversible dehydration kinetics of ammonium, potassium, and other mixed alums. Likewise, with minor variations, Anous et al. (1951) applied these ideas to the dehydration of chrome alum, Ball and Norwood (1973) to the calcium sulfate-water system, Horlock et al. (1963) to the decomposition of magnesium hydroxide, and Gardet et al. (1976) to the dehydration of calcium sulfate dihydrate. Benton and Drake (1934) considered the influence of adsorbed oxygen in the dissociation kinetics of Ag_2O, and Spencer and Topley (1929) considered the influence of adsorbed CO_2 on the decarbonation kinetics of Ag_2CO_3. In all these cases, one adsorption site was considered equivalent to each reaction site.

If one considers a pseudosteady state of the surface coverage of adsorbed water molecules and assumes that the adsorption behavior is Langmuirian in nature, then writing a steady state balance for constant site coverage yields:

$$k_1(1-\theta)P - k_2\theta + k_3(1-\theta)^n = 0 \tag{4}$$

where the first term is the rate of surface filling by adsorption, the second term is the rate of surface emptying by desorption, and the third term is the rate of surface filling by chemical reaction. The third term implies that for nonzero values of n, the rate of chemical reaction is related to the concentration of unoccupied adsorption sites. A value of $n = 1$ implies that one adsorption site corresponds to one reaction site, and a value of $n = 2$ implies that two adsorption sites correspond to one reaction site. For the particular reaction at hand, two adsorption sites correspond to one reaction site; accordingly, $n = 2$. Solving Eq. 4 for θ and obtaining the reaction rate from the third term above yields:

$$r = \frac{k_3}{4}\left\{\left[\left(\frac{k_1P}{k_3}+\frac{k_2}{k_3}\right)^2 + 4\frac{k_2}{k_3}\right]^{1/2} - \left(\frac{k_1P}{k_3}+\frac{k_2}{k_3}\right)\right\}^2 \tag{5}$$

If one or more of k_1P, k_2, or k_3 dominates the remaining terms, the relative influences of adsorption, desorption, and chemical reaction can produce simplified asymptotic cases.

A numerical study was undertaken to clarify how pressure influences the reaction rate in Eq. 5 for the possible ranges in k_1P, k_2, and k_3. For the cases where either $k_1P \gg k_2$ and $k_1P \gg k_3$ or $k_1P \gg k_2$, $k_3 \gg k_2$ and $k_3 \cong k_1P$, the site coverage is very close to 1 for all system pressures and the decomposition rate is given by:

$$r = k_3\left(\frac{k_2}{k_1P}\right)^2 \tag{6}$$

Here, the site coverage is dominated by a strong adsorption character. For the other asymptotic cases, the rate is a more complicated function of pressure; however, as shown in Figure 14 the apparent power dependency of rate on pressure will always be between 0 and -2, changing rapidly between these limits for relatively small changes in k_1P, k_2, or k_3.

In the thermal experiments done here, the water vapor pressure was varied over three orders of magnitude overall and by about one order of magnitude for each temperature. Throughout this span of values, the overall measured kinetics for the second decomposition was found to vary with the water vapor pressure to the power of -2.12 ± 0.17. Clearly, within the associated uncertainty an inverse-squared dependence on the water vapor pressure is indicated. The relative constancy of this exponent with variations in P and T (and therefore in k_1, k_2, and k_3) indicates that the system operates within the lower right region of Figure 14.

As is shown in Figure 13, the velocity of the moving interface between product and reactant phases ranged from about 5×10^{-14} to 3×10^{-11} m/s. Saalfeld (1960) established that the depth of one layer of hexagonally placed aluminum atoms in the gibbsite crystal is near 4.855×10^{-10} m. If one assumes that each hexagonal configuration of aluminums constitutes one site, and that the stoichiometry of the decomposition is well represented by the equation $Al_2O_3 \cdot 3H_2O \rightarrow Al_2O_3 \cdot 0.5H_2O + 2.5H_2O$, one can expect about 8.5×10^{-15} mol H_2O to be evolved per meter of interface advance, per site. Thus, evolution rate of product water vapor ranged from about 4×10^{-28} to 3×10^{-25} mol H_2O/s/site for the experiments here, or from 2.4×10^{-4} to 0.18 molecules H_2O/s/site.

If the rate constants in Eq. 6 are written to show temperature explicitly:

$$r = \frac{k_{20}^2 k_{30}}{k_{10}^2 P^2}\exp -[E_r + 2(E_d - E_a)]/RT \tag{7}$$

The measured value for the activation energy, E_m, is thus:

$$E_m = 2(E_d - E_a) + E_r \tag{8}$$

Since $(E_d - E_a)$ equals the adsorption energy, ϵ,

$$E_m = 2\epsilon + E_r \tag{9}$$

that is, the overall measured activation energy is the sum of the activation energy for the chemical reaction and twice the adsorption energy for the product water vapor. Papee (1958) measured the difference between the adsorption energy and the liquefaction energy, $\epsilon - E_L$, for water vapor adsorbing on these transition alumina, and obtained a value of 8.4 kJ/mol. This value places the adsorption character between the values normally associated with physisorption and chemisorption. Since the liquefaction energy varies from about 36 to 32 kJ/mol over the temperature range of 468 to 508 K used here (Reynolds and Perkins, 1977), the average value for the adsorption energy $\epsilon = 42 \pm 2$ kJ/mol.

A logarithmic representation of the kinetic interface velocity as a function of water vapor pressure is given in Figure 13. An average slope of -2.0 is well within the uncertainty limits given in the previous section. The uncertainties in the data of Figure 13 contain contributions from the uncertainties in the measurements of the decomposition rate, the system water vapor pressure, the boehmite conversion, the degree of hydration of the product alumina, and the slit pore surface area. After choosing an average slope of -2.0 in Figure 13, a least-squares analysis was performed on the data. The value for the overall, measured activation energy was estimated to be 342 ± 15 kJ/mol. Equa-

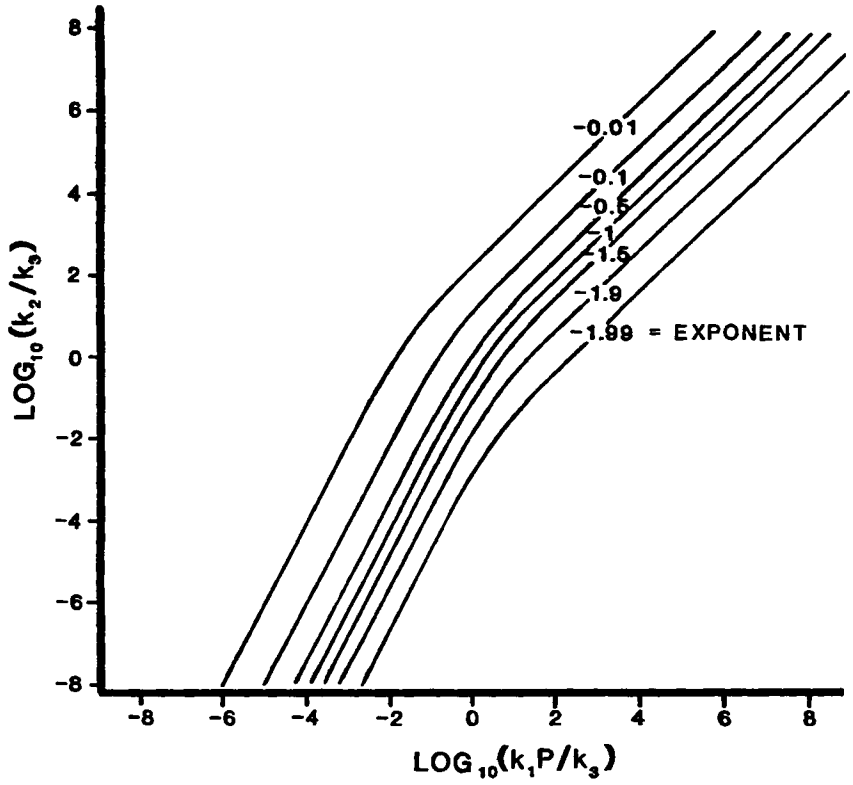

Figure 14. Apparent power dependence of rate on pressure.

tion 9 and the adsorption energy value of 42 ± 2 kJ/mol were used to estimate the value of the activation energy for the chemical decomposition alone. Thus, E_r was estimated to be 260 ± 20 kJ/mol.

Literature reports for the activation energies of decomposing aluminum hydroxides are few. Eyraud and Goton (1954) decomposed hydrargillite, an aluminum hydroxide with the same X-ray diffraction peak locations as gibbsite but with dramatically different intensity ratios, under a controlled, pure water vapor atmosphere. They reported activation energies increasing from 230 kJ/mol at 600 Pa water vapor pressure to 260 kJ/mol at 2,000 Pa. These authors, however, did not make measurements of the reactive area of their decomposing samples, but instead reported overall conversion rates. Since variations in the internal surface area should be expected for their 100 μm particle size samples, their reported trend in activation energy with water vapor pressure must also include this effect. For gibbsite, Rouquerol et al. (1979) noted that in order to maintain the same second decomposition rate when increasing the water vapor pressure from 5 to 133 Pa, the temperature had to be raised by almost 30 K. Extrapolating the model presented here to Rouquerol's reactor conditions yields an apparent activation energy of about 360 kJ/mol, comparing well with the results reported here. Rouquerol also postulated that the desorption of water vapor from the decomposing surface was the rate-determining step.

As noted above, a value of $n = 2$ in the adsorption/reaction model assumes that one reaction site corresponds to two adsorption sites. Rouquerol (1979) estimated the diameters of the microcapillaries to be near 5×10^{-4} μm, slightly larger than the 3.8×10^{-4} μm dia. of the hexagonal aluminum positioning in the reactant phase, and tending to widen somewhat at higher operating vapor pressures. The trend for increasing chemical activation energies with increasing water vapor pressure is perhaps a reflection of this capillary widening, increasing the distances between the opposing hydroxyls and thus inhibiting the condensation. The area of the site at the bottom of the capillary would be near 20×10^{-20} m^2, large enough to accommodate just over one adsorbed nitrogen molecule lying flat (N_2 area = 16.2×10^{-20} m^2) or just about two water molecules lying flat (H_2O area = 10.6×10^{-20} m^2). Comparing nitrogen adsorption measurements with water adsorption measurements has indeed shown that the adsorption capacity on a molar basis is about twice as large for water as it is for nitrogen, even though the two measurements are very close on a volumetric basis, and yield comparable values for the solid's porosity.

If a proton released from the AlO—H structure of an unoccupied site were to form product H_2O with the Al—OH of an adjacent but occupied site, the observed chemical kinetics would be inversely proportional to the water vapor pressure, rather than inversely proportional to the square of this pressure. The implication of the requirement that both adsorption sites be unoccupied is that the adsorbed water acts to strengthen both the Al—O and O—H bonds of the $Al(OH)_3$.

Distribution of slab sizes

It is of some interest to establish how the fracturing of the gibbsite crystals divides the material into an array of parallel slabs joined by internal bridges but open on all sides. The fracturing phenomenon is certainly a consequence of the formation of internal pockets of boehmite in the first decomposition, and

exposes an internal surface against which the conversion to transition alumina proceeds. The interface velocity is constant under constant conditions of temperature and pressure, but given a distribution of slab sizes, as the smaller sizes become fully consumed, the measured decomposition rate will diminish.

The interface velocity defined by Eq. 3 was experimentally obtained via measurements of the long, linear portion of the TGA scan and of the slit pore surface area.

If $f(x)$ is the distribution of slab sizes and $F(x)$ is defined by

$$F(x) = \int_0^x f(x)dx \tag{10}$$

the fraction of the total slab surface area corresponding to full conversion of slabs of sizes less than x is $[1 - F(x)]$. At a given time the reaction interface in the largest slab has traveled a distance rt, and the total length of consumed material in this largest slab is $2rt$. Thus, all slabs of widths less than $2rt$ have already been consumed by time t.

If $C(t)$ is the decomposition rate as measured on the thermal assembly,

$$C(t) = \rho rs[1 - F(x)]. \tag{11}$$

Since $x = 2rt$,

$$F(x) = 1 - \frac{C(x/2r)}{\rho rs} \tag{12}$$

and $f(x)$ can be obtained from Eq. 10.

As an example, the above equations were used to analyze the slab size distribution for a gibbsite sample decomposed at 478 K under 215 Pa water vapor pressure. The resulting slab size distribution is given in Figure 15; it is skewed in the direction of smaller slab sizes and has an average slab size of 850×10^{-4} μm. Approximately 98% of the slabs formed fell into the relatively narrow width range between about 400×10^{-4} μm and $1{,}800 \times 10^{-4}$ μm, reflecting a uniformity in the formation of slit-shaped pores across the macroscopic gibbsite crystals and crystal-aggregated particles. This in turn suggests a rather wide degree of dispersion of the product boehmite of the first decomposition within the gibbsite matrix. Had the boehmite formation been more localized, a much wider distribution of slab sizes would have been expected.

Additionally, the slab size distribution found here seems to correspond well with the observed lower limit for the dimensions of gibbsite particles required for boehmite formation to occur at all. For similar reactor conditions, Tertian and Papee (1958) reported no formation of boehmite in gibbsite crystals below $1{,}000 \times 10^{-4}$ μm, while Rouquerol et al. (1975) reported miniscule boehmite formation in gibbsite crystals with an average diameter of $2{,}000 \times 10^{-4}$ μm. For crystals of average diameter $10{,}000 \times 10^{-4}$ μm, they reported boehmite conversions of about 7% for slow heating at 270 Pa water vapor pressure. Thus, the fracturing of the gibbsite crystals appears to cause the end of the first decomposition by producing new gibbsite microcrystals too small to allow for further boehmite formation.

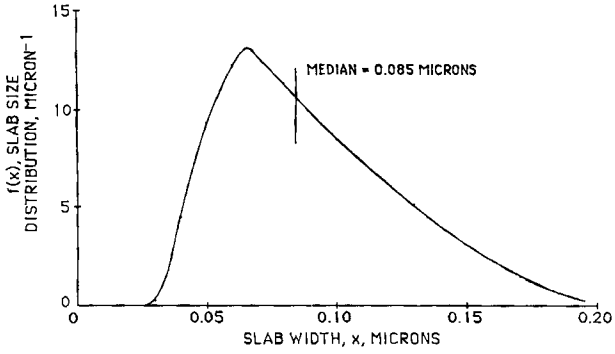

Figure 15. Slab size distribution for fissured aluminum hydroxide.

Notation

$C(t)$ = decomposition rate, s^{-1}
c = linear decomposition rate, s^{-1}
E_a = activation energy for adsorption, kJ/mol
E_d = activation energy for desorption, kJ/mol
E_L = liquefaction energy, kJ/mol
E_m = measured activation energy, kJ/mol
E_r = activation energy for reaction, kJ/mol
$F(x)$ = cumulative slab site distribution
$f(x)$ = slab size distribution, μm^{-1}
k_1 = adsorption rate constant, mol/s · Pa
k_{10} = adsorption rate constant preexponential factor, mol/s · Pa
k_2 = desorption rate constant, mol/s
k_{20} = desorption rate constant preexponential factor, mol/s
k_3 = reaction rate constant, mol/s
k_{30} = reaction rate constant preexponential factor, mol/s
n = surface reaction order
P = pressure, Pa
P_o = saturated vapor pressure, Pa
p = percent conversion
R = gas constant, kg · m^2/kmol · s^2 · K
r = rate of chemical, mol/s
r_k = Kelvin radius, m
S = slit pore area, m^2/g $Al(OH)_3$ initially
s = slit pore area, m^2/g $Al(OH)_3$ not converted to boehmite
T = temperature, K
t = time, s
V_m = adsorbate molar volume, m^3/kmol
v = interface velocity, m/s
x = slab thickness, μm

Greek letters

α = adsorbate wetting angle
γ = adsorbate surface tension, kg/s^2
ϵ = adsorption energy, kJ/mol
θ = surface coverage
ρ = gibbsite density, g/m^3 or $g/\mu m^3$

Literature cited

Acock, G. P., W. E. Garner, J. Milsted, and H. J. Willavoys, "The Dehydration of Ammonium, Potassium, and Some Mixed Alums," *Proc. Roy. Soc. London*, **A189**, 508 (1947).

Anous, M. M. T., R. S. Bradley, and J. Colvin, "The Rate of Dehydration of Crome Alum," *J. Chem. Soc.*, 3348 (1951).

Arakelyan, O. I., and A. A. Chistyakova, "Investigation of Synthetic Boehmite," *J. Appl. Chem. USSR in English Trans.*, **35**(7), 1396 (1962).

Ball, M. C., and L. S. Norwood, "Studies in the System Calcium Sulphate/Water. 4: Rehydration of Hexagonal $CaSO_4$," *Chem. Soc. London, J. Faraday Trans I*, **69**, 169 (1973).

Barrett, E. P., L. G. Joyner, and P. P. Halenda, "The Determination of Pore Volumes and Area Distributions in Porous Substances. I: Computations from Nitrogen Isotherms," *J. Am. Chem. Soc.*, **73**, 373 (1951).

Benton, A. F., and L. C. Drake, "Kinetics of Reaction and Adsorption in the System Silver-Oxygen," *J. Am. Chem. Soc.*, **56,** 255 (1934).

Brindley, G. W., J. H. Sharp, J. H. Patterson, and B. N. Narahari Achar, "Kinetics and Mechanism of Dehydroxylation Processes. I: Temperature and Vapor Pressure Dependence of Dehydroxylation of Kaolinite," *Am. Minerologist,* **52,** 201 (1967a).

Brindley, G. W., B. N. Narahari Achar, and J. H. Sharp, "Kinetics and Mechanism of Dehydroxylation Processes. II: Temperature and Vapor Pressure Dependence of Dehydroxylation of Serpentine," *Am. Minerologist,* **52,** 1697 (1967b).

Calvet, E., and H. Thibon, "Thermocinetique de la Decomposition Thermique Menagee de Divers Trihydrates d'Alumine," *Bull. Soc. Chim. France,* 1342 (1954).

Courtial, R., Y. Trambouze, and M. Prettre, "Influence des Conditions du Traitment sur la Teneur en Bochmite des Products de Deshydration Partielle de l'Hydragellite," *Comptes Rendus,* **242,** 1607 (1956).

deBoer, J. H., "The Shape of Capillaries," *Structure and Properties of Porous Materials: Colston Papers,* D. H. Evertt and F. S. Stone, ed., Butterworths, London, 68 (1958).

deBoer, J. H., J. M. H. Fortuin, and J. J. Steggerda, "The Dehydration of Alumina Hydrates. I," *Proc. Konin. Ned. Akad. Van Wetensch., Ser. B,* **57,** 170 (1954a).

———, "Part II," *ibid.,* **57,** 434 (1954b).

———, "Part III," *ibid.,* **59,** 435 (1956).

deBoer, J. H., and B. C. Lippens, "Studies on Pore Systems in Catalysis. II," *J. Catal.,* **3,** 38 (1964a).

———, "IV: The Two Causes of Reversible Hysteresis." *ibid.,* **3,** 268 (1964b).

Eyraud, C., and R. Goton, "Etude Cinetique de la Dissociation Thermique d'Hydrates d'Alumine," *J. de Chim. Phys.,* **51,** 430 (1954).

Gardet, J. J., B. Guilhot, and M. Souatelle, "The Dehydration Kinetics of Calcium Sulfate Dihydrate, Influence of the Gaseous Atmosphere and the Temperature," *Cement Concrete Res.,* **6,** 697 (1976).

Gilliand, E. R., R. F. Baddour, and J. L. Russell, "Rates of Flow through Microporous Solids," *AIChE J.,* **9**(1), 90 (1958).

Horlock, R. F., P. L. Morgan, and P. J. Anderson, "Effects of Water Vapor on the Decomposition of Magnesium Hydroxide," *Trans. Faraday Soc.,* **59,** 721 (1963).

Laubengayer, A. W., and R. S. Weisz, "A Hydrothermal Study of Alumina-Water Equilibria," *J. Am. Chem. Soc.,* **65,** 247 (1943).

Lippens, B. C., B. G. Linsen, and J. H. deBoer, "Studies on Pore Systems in Catalysts. I: The Adsorption of Nitrogen—Apparatus and Calculation," *J. Catal.,* **3,** 32 (1964).

Morgan, J., and B. E. Warren, "X-ray Analysis of the Structure of Water," *J. Chem. Phys.,* **6,** 666 (1938).

Omata, H., and L. Brown, "Using the Dusty Gas Equation in Catalyst Pores Smaller than 50Å Radius," *AIChE J.,* **18**(5), 967 (1972.)

Papee, D., "Adsorption d'Eau et Rehydration des Alumines Activees," *Comptes Rendues de l'Academie des Sciences,* **246,** 2377 (1958).

Papee, D. and R. Tertian, "Etude de la Decomposition Thermique de l'Hydrargillite et de la Constitution de l'Alumine Activee," *Bull. Soc. Chim. France,* 983 (1956.)

Pauling, L., *The Nature of the Chemical Bond,* Cornell Univ. Press, Ithaca, NY (1960).

Rao, M., and J. M. Smith, "Diffusion Resistances in Alumina and Silica Catalysts," *AIChE J.,* **9**(4), 485 (1963).

Reynolds, W. C., and H. C. Perkins, *Engineering Thermodynamics,* 2nd ed., McGraw-Hill, New York (1977).

Rouquerol, A., F. Rouquerol, and M. Ganteaume, "Thermal Decomposition of Gibbsite under Low Pressures. I: Formation of the Boehmite Phase," *J. Catal.,* **50,** 99 (1975).

———, "II: Formation of Microporous Alumina," *ibid.,* **57,** 222 (1979).

Saalfeld, H., "Strukturen des Hydrargillits und der Zwischenstufen usw.," *Neues Jahrb. Mineral. Abh.,* **95,** 1(1960).

Sato, T., "The Dehydration of Alumina Trihydrate," *J. Appl. Chem.,* **9,** 331 (1959).

Scott, B. A., and W. H. Horsman, "Structural Changes During the Production of Corundum by Calcination of Gibbsite and Their Influence on Fabrication," *Trans. Brit. Ceram. Soc.,* **69**(2), 37 (1970).

Sohn, H. Y., and J. Szekely, "A Structural Model for Gas-Solid Reactions with a Moving Boundary. III: A General Dimensionless Representation of the Irreversible Reaction between a Porous Solid and a Reactant Gas," *Chem. Eng. Sci.,* **27,** 763 (1972).

Spencer, W. D., and B. Topley, "Chemical Kinetics of the System Ag_2CO_3 $Ag_2O + CO_2$," *J. Chem. Soc.,* 2633 (1929).

Tertian, R., and D. Papee, "Etude aux Rayon X des Products Resultant de la Deshydration Menagee de l'Hydrargillite et de la Bayerite," *Comptes Rendues de l'Academie des Sciences,* **236,** 1565, (1953a).

———, "Sur les Proprietes de Rehydration des Products Obtenus par Decomposition Thermique de l'Hydrargillite et de la Bayerite," *ibid.,* 1668 (1953b).

———, "Transformations Thermique et Hydrothermique de l'Alumine," *J. Chim. Phys.,* **55,** 341 (1958).

Tertian, R., D. Papee, and A. Charrier, "Etude aux Rayons X des Alumines Anhydres de Transition," *Comptes Rendues de l'Academie des Sciences,* **238,** 98 (1954).

Torkar, K., H. Egghart, H. Krischner, and H. Worel, "Influence of Sodium on the Formation and the Thermal Decomposition of Bayerite," *Monatsh. Chem.,* **92,** 525 (1961).

Washburn, E. W., ed., *International Critical Tables of Numerical Data: Physics, Chemistry and Technology,* McGraw-Hill, New York **3,** 368 (1928).

Wefers, K., and G. M. Bell, "Oxides and Hydroxides of Aluminum," *Alcoa Res. Lab., Tech. Paper No. 19* (1972).

Young, D. A., *Decomposition of Solids,* Pergamon, Oxford and New York (1966).

Manuscript received May 6, 1985, and July 10, 1985, and revision received Jan. 13, 1986.